Simulating Ocean Wave Movement in a Soft Pneumatic Surface

Alexandra W. Steelman, Elena B. Sabinson, Isha Pradhan, Aratrika Ghatak, and Keith E. Green,
Senior Member, IEEE

Abstract— **It is well understood that nature has a calming effect on us. But in a physical space remote from nature, might the robotic embodiment of a natural phenomenon have the same effect? To address this question, we have simulated the soothing movement of ocean waves in a soft robotic surface, both as a simulation and in a physical prototype. In this paper, we report on our modeling methods of this natural phenomenon, we present the application of a selected model to both a simulation of the predicted inflation pattern of the soft robot surface and to the physical soft robot surface, and we compare the behavior of the physical robot to our simulation as a means to validate our design. We observed that the prototype's frequency spectrum successfully shared the general trend and shape as our mathematical model. This research introduces a novel robot for a novel application: a soft robot to promote restoration and help regulate mental wellbeing in tight physical confines.**

I. INTRODUCTION

Natural environments have many positive effects on human health, such as improving mood and reducing stress [1], [2]. Specifically, visual exposure to scenes of nature have been shown to have significantly positive effects on stress compared to urban scenes [3]. But in a physical space remote from nature, might the robotic embodiment of a natural phenomenon have the same effect? Our goal is to translate natural phenomena through the robotic surface (Fig. 1) to calm us, as we explored in our pilot study with an early prototype of the kind presented in this paper with a small sample of human participants interacting with it, as reported in [4].
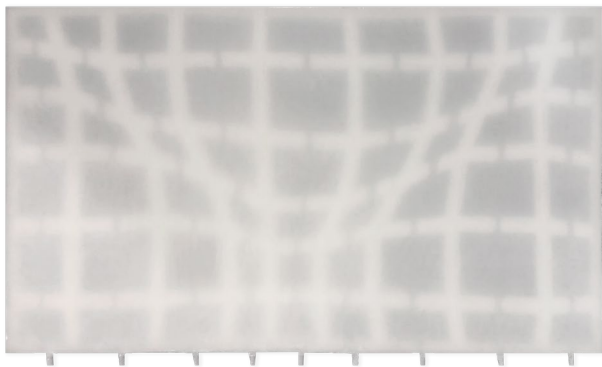

Figure 1.   A 33" x 18", 9-channel prototype with one air inflow point to each channel.
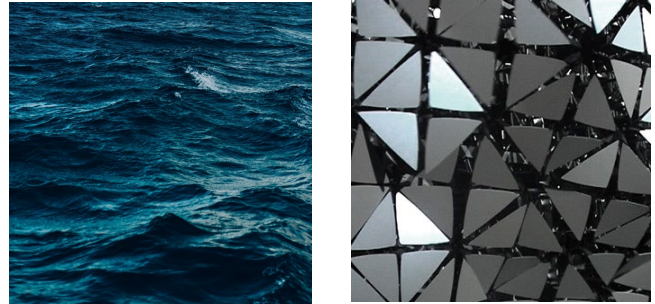
Figure 2.   *Left*—Gentle ocean waves; *Right*—Hyposurface

This paper discusses simulating and modeling ocean waves into an inflation pattern, providing a visual representation of nature for inhabitants of confined, urban spaces with little access to real nature. A brief video demonstrates the current prototype (https://bit.ly/iros21). The Attention Restoration Theory [5] states that natural patterns can have a restorative effect such as improving our ability to concentrate. This is facilitated through exposure to pleasing stimuli that only requires Soft Fascination rather than Directed Attention [6]. Our aim is to translate this soothing ocean phenomenon into a novel soft robotic surface that can evoke a sense of Soft Fascination. The design that we use for our prototype builds upon a previous soft robotic surface that involves inflation through air channels in the surface [4]. Our physical prototype, depicted in Fig. 1 adds additional channels and is a physically larger surface, allowing more room for a pattern translation and more interaction with the prototype. We explore several different methods to represent gentle ocean wave movement as seen in Fig. 2, including various sum of sines models, sampling from ocean displacement data and the Pierson-Moskowitz spectrum and Mitsuyasu Angular Distribution.

II. RELATED WORK

Current implementations of visualizing a pattern through a robot surface involve a direct implementation of an algorithm onto the surface. The rigid-link HypoSurface (Fig. 2) uses a large number of linear actuators, each actuator imparting control to the eight rigid "pixels" connected to it. [7]. We take a different approach, in a soft robot, limiting the number of parts required for implementing the pattern. Instead of direct control over each part of the surface, we have a constraint of a maximum of two pressure regulators feeding a nonuniform

Alexandra W. Steelman is with the School of Civil and Environmental Engineering, Cornell University, Ithaca NY 14853 USA (aws226@cornell.edu).

Elena B. Sabinson, is with the Departments of Design & Environmental Analysis, Cornell University, Ithaca NY 14853 USA (es963@cornell.edu).

Isha Pradhan was with the Sibley School of Mechanical and Aerospace Engineering, Cornell University, Ithaca NY 14853 USA (ip94@cornell.edu).

Aratrika Ghatak is with the School of Electrical and Computer Engineering, Cornell University, Ithaca NY 14853 USA (ag9886@cornell.edu).

Keith E. Green, Departments of Design & Environmental Analysis and the Sibley School of Mechanical and Aerospace Engineering, Cornell University, Ithaca NY 14853 USA (keg95@cornell.edu).

grid of cells organized as nine "channels" where the cells within an individual channel are connected. This design adds an additional layer of complexity to our pattern, enabling us to build upon the previous work of our lab on robotic surfaces [8], [9], explored through a new form and materiality capable of more granular movement.

Another approach to embodying patterns of motion in a robotic surface is found in the Haptic Jamming display [10], a soft robot surface that controls shape through particle jamming cells and pressurizing an air chamber beneath the surface. While the control of the shape of this display is by a person pressing on its surface, we focus instead on controlling shape through inflation pattern applied to the surface. Another robotic embodiment of patterns is the ExoBuilding [11], something of a small, camping tent that physically swells as controlled by the physiological data of its inhabitant [11]. Our surface is not an environment like the ExoBuilding, but rather a robot surface that we envision installed in confined environments like a micro-office or home, or a submarine, spacecraft or other capsule habitat, in which the physical embodiment of gentle ocean waves provides a calming effect.

There are many different mathematical ocean wave models that we considered for creating our inflation pattern. One such model of waves on a water surface follows a Stokes solution and sinusoidal wave theories [12]. We ultimately decided not to use this model because it required more complexity than needed to create an inflation pattern for the surface. Instead, we characterized ocean movement in the frequency domain, applying previously developed idealized ocean wave spectra in our mathematical model [13].

III. SYSTEM DESCRIPTION

Due to our limited number of pressure regulators, our mathematical model consisted of standing waves, as more pressure regulators would have been needed to model a traveling wave. Instead of directly translating our model to the prototype movement, we utilized a creative and biomimetic approach in the implementation of our model by having a nonuniform grid for our prototype. The geometry was created in Grasshopper (grasshopper3d.com) by following features of a bitmap nature image as we developed in our early soft robotic surface as reported in [4]. Our cell sizes were irregular which created additional variation in the physical prototype movement. For the final mathematical model, we generated a finite sum approximation in MATLAB (mathworks.com) for each regulator and added that into our Arduino (arduino.cc) code to input to the prototype. The design and programming of our pressure regulator system draws on the earlier work from our lab led by Jessica Merino [15].
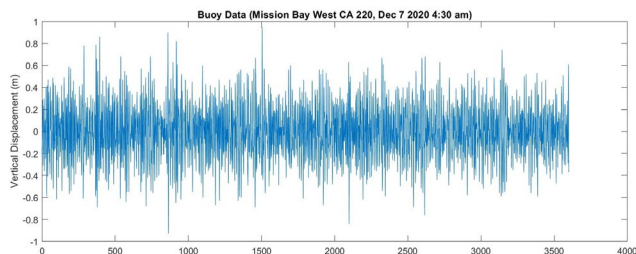
Figure 3.   Vertical displacement buoy data collected at Mission Bay West CA on December 7, 2020 between 4:30 am and 5:00 am.
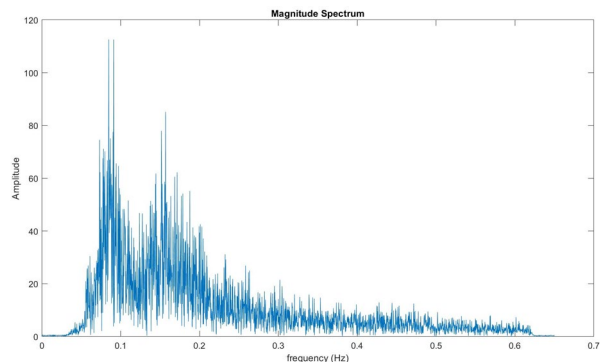
Figure 4.   Magnitude spectrum of buoy data collected at Mission Bay West CA on December 7, 2020 between 4:30 am and 5:00 am.
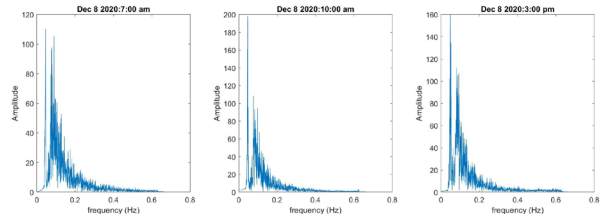
Figure 5.   Fourier transforms of buoy data collected from Mission Bay West on December 8, 2020 at 7:00 am, 10:00 am, and 3:00 pm from left to right.

IV. METHODS

To characterize ocean wave movement through a mathematical model, we first analyzed real, deep ocean wave data in both the time and frequency domain. Utilizing data from The Coastal Data Information Program [16] which publishes real time ocean data from different buoy locations, we plotted the time series as well as the corresponding frequency spectrum of a few chosen data sets. Ultimately, the time series of the buoy data, as shown in Fig. 3 did not tell us much about the specific characteristics of ocean wave data. At a glance, it appears random, resembling white noise. The Fourier transform (Fig. 4) was, however, very helpful as it offered a more specific shape. We also took the Fourier transform of a few other data sets and identified an obvious trend in their magnitude spectra as shown in Fig. 5. After analyzing multiple sets of ocean wave magnitude spectra, we decided to focus on the underlying frequencies that define ocean wave movement.

As a result, our approach in modeling ocean wave movement rests on the fact that an ocean wave can be interpreted as an infinite number of simple harmonic waves of different amplitudes, frequencies, and directions of propagation. In terms of a 2D wave, this can be:

$$u(x,t) = \Sigma_{n=1}^{N} A_n * cos(k_n X_n + w_n t + \phi_n) \tag{1}$$

where:

$$A_n = \text{Amplitude}$$
$$k_n = \text{wave number}$$
$$w_n = 2\pi \frac{1}{T} = \text{angular frequency}$$
$$\phi_n = \text{phase}$$

Since this is a complex model, we applied ocean wave spectra to describe this infinite sum.

In order to understand the distribution of these parameters in ocean waves, various idealized ocean spectra have been constructed. The total direction ocean wave spectra is represented by the energy spectrum, $E(f)$, and the angular distribution, $D(f,\theta)$, as shown in (2).

$$E(f,\theta) = E(f) * D(f,\theta) \qquad (2)$$

We then used this total directional ocean wave spectrum as a filter which we passed through white noise to create the resulting 2D ocean wave surface time series.

To construct the total directional ocean spectrum, we first had to construct each of its components. For the energy spectrum, we decided to utilize the Pierson Moskowitz Spectrum, as it is one of the most commonly used ideal spectra for deep water ocean waves, and it has the added benefit of being relatively simple [13]. The spectrum is based on the understanding that wind blows over a wide sea surface for a long period of time, such that the ocean surface is in a state of equilibrium with the wind. Thus, by using this idealized spectrum (3), we can construct the model for different wind velocities. This is a point of interest for the qualitative aspects of the projects as different wind velocities can be mapped to emotional states to promote unique calming effects for a human user in response to the intensity of their emotion.

$$E_{PM}(f) = \frac{ag^2}{(2\pi)^4 f^5} * exp(\frac{-5}{4}(\frac{f_m}{f})^4)$$

$$f_m = \frac{0.13g}{v} \qquad (3)$$

where α is 0.0081, v is the wind velocity, g is the acceleration of gravity, f is frequency, and f_m is peak frequency.

It is important to note this spectrum also allows us to define the dispersion which is the relationship between wavelength, frequency, and gravity. For deep water waves the dispersion relationship is:

$$w^2 = 2\pi g/L \qquad (4)$$

In Fig. 6 we see the general trend that as the wind velocity increases the energy distribution shifts to lower frequencies with higher energy. This tells us that high winds result in an
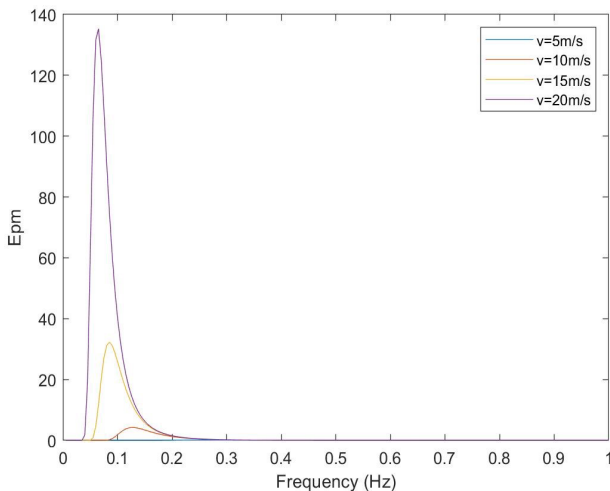

Figure 6. Pierson Moskowitz Energy Spectrum for varying wind conditions.

ocean surface comprised of simple harmonics with lower frequencies and higher amplitudes than that of an ocean surface in low wind conditions.

For the angular distribution we applied the Mitsuyasu Distribution which was constructed as an addition to the Pierson Moskowitz Spectrum in order to represent the total directional ocean wave spectrum. This model describes the spreading direction of waves of frequency, f, propagating under an angle θ relative to the direction of the wind. The shape of this angular distribution is described in (5) [17].

$$D(f,\theta) = \frac{\Gamma(s+1)}{2\sqrt{\pi}\Gamma(s+0.5)} * (cos^2\frac{\theta}{2})^s$$

$$\Gamma(s+1) = \int_0^\infty x^s e^{-x} dx$$

$$s = \begin{cases} 9.77 * \frac{f}{f_m}^{-2.5} & f \geq f_m \\ 6.97 * \frac{f}{f_m}^5 & f < f_m \end{cases} \qquad (5)$$

where f is frequency, f_m is the peak frequency, θ is the angle relative to the wind direction, and s controls the concentration of the function.

The result of multiplying these spectra is the total directional energy spectrum as a function of wind velocity (Fig. 7), where increasing velocity shifts the energy distribution to lower frequencies and higher energy. White noise was filtered, and the inverse Fourier transform was taken
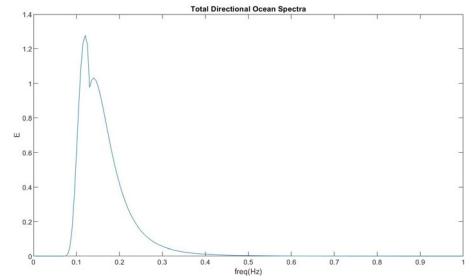

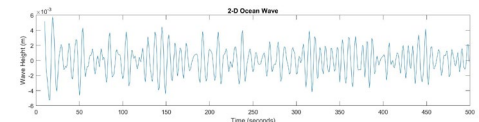Figure 7. Total directional spectrum with v=10m/s and $\theta = \pi/3$.

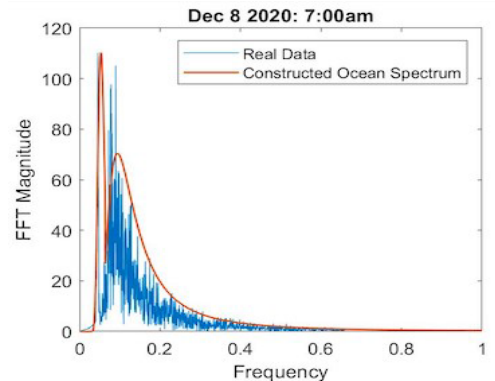Figure 8. Resulting 2D Ocean Surface

Figure 9. A comparison of the total directional spectrum to the Fourier transformations of the buoy data.

to get the final 2D surface ocean time series (Fig. 8). In Fig. 9, we see the constructed total directional ocean wave spectrum, treated as a function of wind velocity and relative angle, is able to closely fit the data collected at Mission Bay West.

As stated previously, the total directional ocean spectrum is based on the fact that we can interpret an ocean surface as an infinite sum of harmonics with different amplitudes, frequencies, and directions of propagation. However, to implement this model onto the system of pressure regulators, we need to find a finite approximation of this infinite sum. Moreover, since we are limited by the number of pressure regulators we have to control our surface, we can further simplify the 2D ocean wave model in (5), which shows a traveling wave, to a standing wave equation comprised of a finite summation of simple harmonics:

$$u(t) = \sum_{n=1}^{N} A_n cos(2\pi f_n t - \phi) \tag{6}$$

where N = the number of harmonics in our finite sum. This equation acts as the input for each pressure regulator. Since we are working with only three pressure regulators, we are able to use a simple phase shift applied to a standing wave rather than inputting spatial coordinates in addition to time as needed for a traveling wave. The latter method however would be more necessary if we were working with a larger number of regulators and therefore more degrees of freedom in our system. As a result, we would need to define a coordinate system and location for each pressure regulator to input spatial coordinates into a traveling wave equation. To choose the set of N amplitude and frequency values, we utilized the "findpeaks" command in MATLAB. After constructing a magnitude spectrum by filtering white noise with the total ocean spectra, selected frequency and amplitude values were taken from the resulting peaks (Fig. 10).

V. Simulation

Using MATLAB, we simulated our mathematical model to tune parameters and predict the resulting surface movement produced by the prototype's geometry and pressure regulator input assignments. Prior to testing, we had to determine key details related to the implementation of our determined mathematical model onto the physical prototype. One of the most apparent obstacles was our limited number of pressure regulators and, therefore, a limited number of degrees of freedom. This was accounted for when developing our mathematical model, creating a sum of simple harmonics made of standing waves rather than traveling waves. We were constrained to using only two pressure regulators which
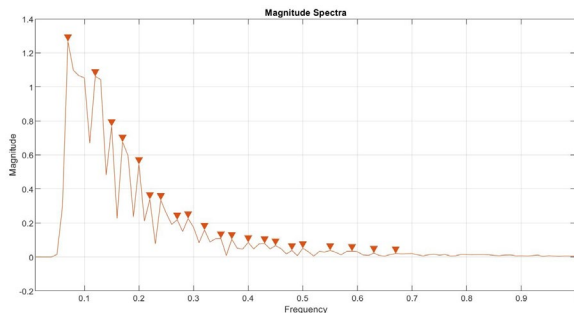

Figure 10.   Location of values collected from "findpeaks" command in MATLAB.
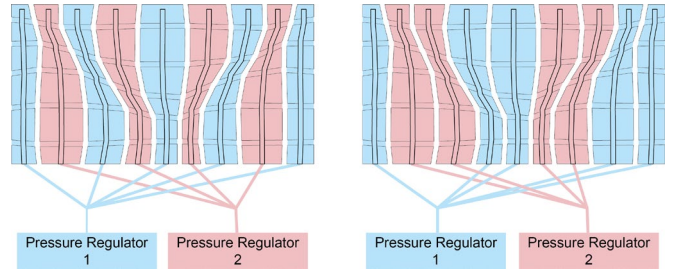

Figure 11.   Two possible pressure regulator assignment configurations.

limited the number of possible tubing configurations between the regulators and nine-channel prototype. We focused on the two pressure regulator assignment configurations shown in Fig. 11. We denote the assignment configuration on the left as "pattern A" and the configuration on the right as "pattern B." The numerical assignments for each regulator as a function of time is shown in (7) and (8). For future testing, we will explore more of these combinations to further evaluate the effect the tubing configuration has on the resulting surface movement.

$$\text{Pressure Regulator 1:} \qquad \sum_{n=1}^{N} A_n cos(2\pi f_n t_{i-1}) \tag{7}$$

$$\text{Pressure Regulator 2:} \qquad \sum_{n=1}^{N} A_n cos(2\pi f_n t_i) \tag{8}$$

In addition to the air channel assignments of our two pressure regulators, we also used the simulation to (a) predict any necessary scale factors, and (b) to confirm that all output values from our mathematical model could be read by the pressure regulators. As a result, we added two parameters to our mathematical model before implementing it in our code, a scale factor, and a bias. The scale factor can be easily approximated by first defining a maximum allowable pressure which is dependent on the prototype being tested. In order to ensure the standing wave equation does not exceed this value, we can multiply the finite sum approximation by the ratio of maximum allowable pressure over twice the maximum amplitude value.

VI. Results

We tested the prototype applying a wind velocity of 8 m/s and a θ value of $\pi/4$ when constructing our finite sum approximation. We also tested for wind conditions of 2 m/s and 4 m/s, but the prototype surface was not able to successfully model these behaviors. This was most likely due to the response rate of the pressure regulators which receive new information at a lower frequency than the frequency range of the wave model for lower wind conditions. As shown in Fig. 6, the frequency spectrum shifts towards higher frequencies for lower wind velocities. For future implementations of natural phenomena onto the surface, further investigation into the frequency range able to be communicated through the pressure regulators will be imperative to understanding in initial constraints when developing our mathematical model.

Our experimental results satisfy both qualitative goals (i.e., the Fig. 13: Comparison of moments captured during testing applying pressure regulator pattern B with simulation from MATLAB movement of our prototype does offer the viewer
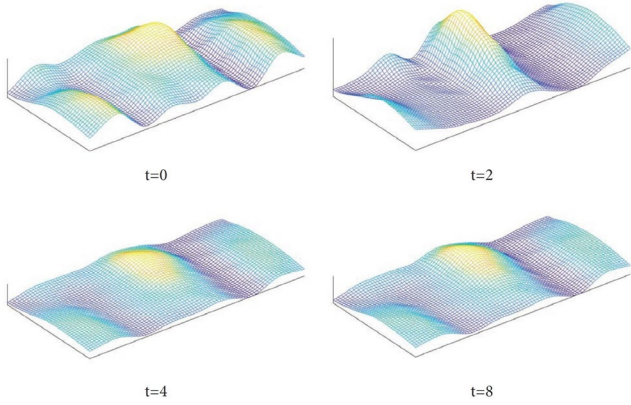
Figure 12.   Predicted inflation of the prototype at four different time steps in the simulation for wind velocity=8 m/s and θ=π/4.

an impression of an ocean surface), as well as quantitative goals (i.e., a validation based in the underlying frequencies the surface exhibits). These two goals are closely interconnected, as we hope to demonstrate that the success of our quantitative goals corresponds to qualitative success and vice versa.

In our experimental validation, we specifically analyzed the resulting movement of the surface from these two types of approaches, first looking at the inflation patterns created and then collecting the frequency spectrum of the surface. We tested pressure regulator patterns A and B as shown in Fig. 11. As seen in Fig. 13, we captured moments during testing when applying pressure regulator pattern B and compared the inflation patterns with the predicted simulation from MATLAB. We observed that while the surface created many of the same inflation patterns we saw in the simulation, it also demonstrated some characteristics that were unexpected. These differences in our predicted model and our prototype
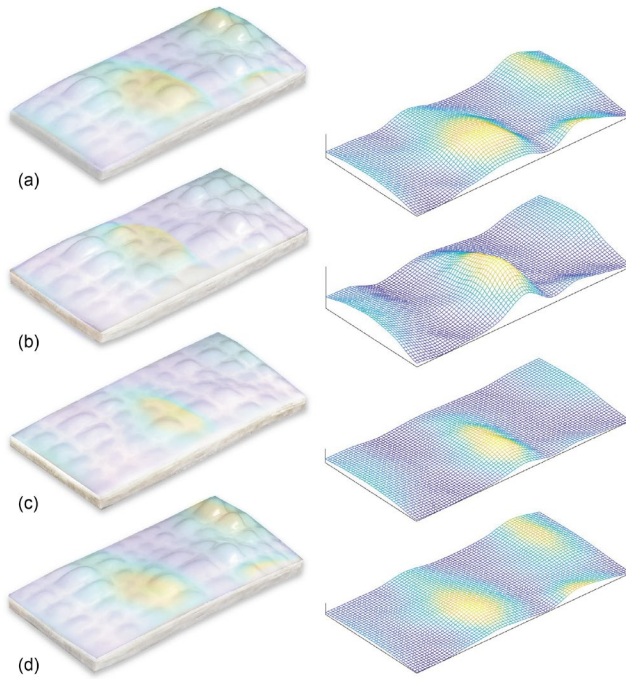
were very helpful in (a) gaining a better understanding of how the size of cells impact the airflow in the prototype, and (b) revealing intrinsic features of our physical prototype that we will take into consideration when iterating the design.

Comparisons showed that the cellular pattern within each channel had a substantial effect on the behavior of the air when input to the prototype. Channels with smaller cells near the input, behaved differently than channels with larger cells first in the array sequence. We observed that air became trapped in some of the larger cells creating a different surface topography than our simulation. In some instances, it appeared as though the inflation occurred at the same time as the simulation, but the inflation peaks were shifted over along the horizontal axis of the surface due to the design constraints of the prototype.

To calculate the resulting frequency of the surface, we took a video of the prototype set at eye level which captured the surface at a rate of 30 frames per second (Fig. 14). To compare the resulting frequencies of the surface with the intended frequency spectrum of the finite sum approximation applied in the Arduino code, we focused on the displacement due to a single pressure regulator which we only connected to the center three air channels. This provided a clear and uniform movement that we could use to take a time series using video frames. We then sampled the 200 frames at a rate of 2 Hz, measuring the total distance from the base of the surface, denoted by the red dotted line in Fig. 14, to the maximum displacement which occurred consistently at the largest cell in the center channel.

From the resulting frequency spectrum shown in Fig. 15, we observed that the prototype's frequency spectrum successfully shared the same general trend and shape as our mathematical model. Moreover, our system was able to capture many of the key frequencies. As seen in Fig. 15, our prototype and constructed ocean wave spectra share frequencies 0.14 Hz, 0.20 Hz, 0.28 Hz, 0.34 Hz, and 0.48 Hz.

Figure 13.   Comparison of moments captured during testing applying pressure regulator pattern B with simulation from MATLAB.
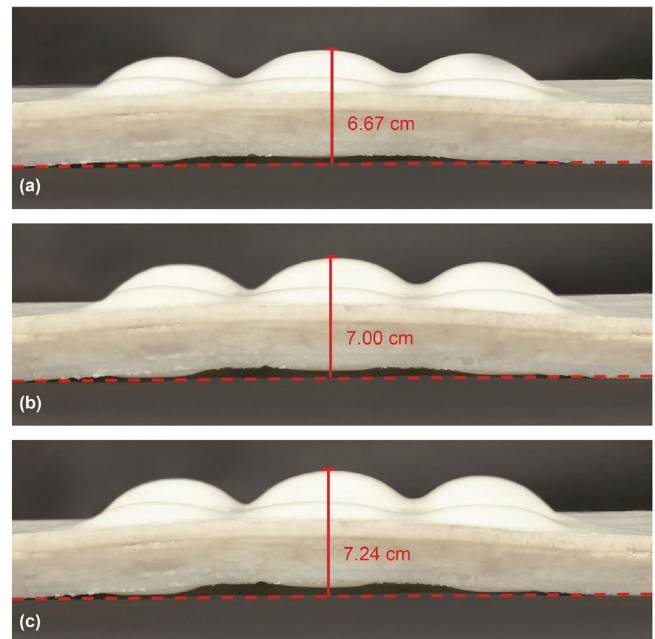

Figure 14.   Three consecutive frames sampled at 2 Hz from video taken at eye level.

The other smaller peak frequencies in Fig. 15 (a), for example, 0.12 Hz, 0.18 Hz, 0.22 Hz, etc. still show the same tendencies as peak frequencies seen Fig. 15 (b) and were likely due to small measurement errors and continuous shifts towards the intended frequencies with a larger sample size. Both spectra gradually decrease in magnitude, with high magnitudes near 0.20 Hz, and lower magnitudes as they near 1 Hz. However, a noticeable difference between the spectra was seen in the large spike at 0.6 Hz in Fig. 15 (a) which was not present in Fig. 15 (b). This low frequency spike could be due to the increased sensitivity that comes with a smaller sample size.

VII. Future Work & Contribution

Our team focused on modeling ocean waves in an inflation pattern with our soft robotic surface and simulating the predicted movement in MATLAB. We plan to extend human user studies with the prototype that we began in [4] to assess (a) how users perceive the relationship between the movement of the prototype and video of real ocean waves, and (b) to determine what velocity of ocean wave movement in the prototype people find the most soothing and restorative.

We designed an irregular grid pattern to mimic patterns in nature, often comprised of geometry with both complexity and order [18]. After this testing period we are better able to control the irregularity of the pattern to achieve desired inflation behaviors to mirror the movement of natural phenomena. We will leverage these findings to guide our development of more biomimetic algorithms of other natural phenomena (e.g., leaves blowing in the wind or the rhythm of rainfall) represented through the behavior of our surface.
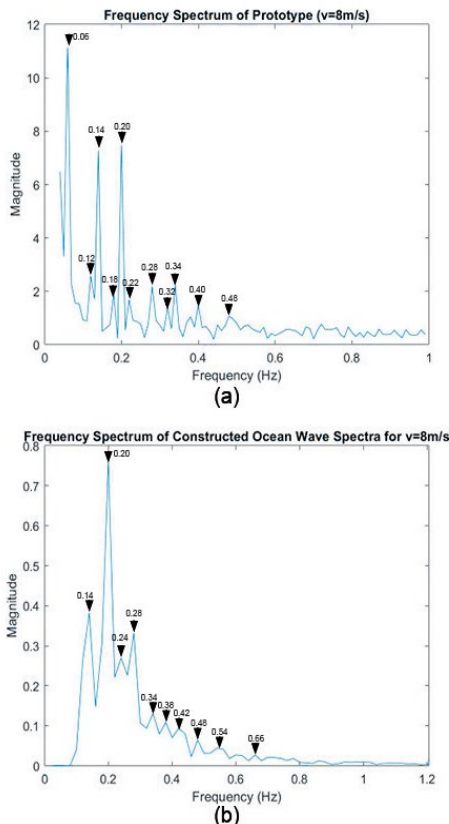

Figure 15. (a) Resulting frequency spectrum of prototype; (b) Frequency spectrum of the constructed finite sum L;'

Future work will also explore different intrinsic designs, including other ways to distribute air within the prototype through variations in air channel configurations. Additionally, we plan to increase the number of pressure regulators, allowing more complexity in inflation patterns and the modeling of complex circular waves or waves originating from point sources. This research introduces a novel robot for a novel application: a soft robot as a means to regulate mental wellbeing in tight physical confines.

VIII. Acknowledgment

IX. References

[1] M. G. Berman et al., "Interacting with nature improves cognition and affect for individuals with depression," *Journal of Affective Disorders*, vol. 140, no. 3, pp. 300–305, Nov. 2012

[2] R. Berto, "The role of nature in coping with psycho-physiological stress: a literature review on restorativeness," *Behavioral Sciences*, vol. 4, no. 4, pp. 394-409, Oct. 2014, doi: 10.3390/bs4040394.

[3] R. S. Ulrich, "Natural Versus Urban Scenes: Some Psychophysiological Effects," *Environment and Behavior,* vol. 13, no. 5, pp. 523–556, Sep. 1981

[4] E. Sabinson, I. Pradhan, and K. E. Green, "Plant-Human Embodied Biofeedback (pheB): A Soft Robotic Surface for Emotion Regulation in Confined Physical Space," in *Proceedings of the Fifteenth International Conference on Tangible, Embedded, and Embodied Interaction*, Feb. 2021, doi: 10.1145/3374920.3375007.

[5] S. Kaplan, "The restorative benefits of nature: Toward an integrative framework," *Journal of Environmental Psychology,* vol. 15, no. 3, pp. 169–182, Sep. 1995, doi: 10.1016/0272-4944(95)90001-2

[6] A. Basu, J. Duvall, and R. Kaplan, "Attention Restoration Theory: Exploring the Role of Soft Fascination and Mental Bandwidth," *Environment and Behavior*, vol. 51, pp. 1055–1081, Nov. 2019.

[7] M. Goulthorpe, M. Burry and G. Dunlop, "Aegis Hyposurface©: The Bordering of University and Practice", *ACADIA*, pp. 344-349, 2001.

[8] R. Sirohi, Y. Wang, S. Hollenberg, I. S. G. Keith, I. D. Walker, and E. Green, "Design and Characterization of a Novel, Continuum-Robot Surface for the Human Environment," in 2019 IEEE 15th International Conference on Automation Science and Engineering (CASE), Vancouver, BC, Canada, Aug. 2019, pp. 1169–1174.

[9] Y. Wang, C. Frazelle, R. Sirohi, L. Li, I. D. Walker, and K. E. Green, "Design and Characterization of a Novel Robotic Surface for Application to Compressed Physical Environments," in *2019 International Conference on Robotics and Automation* (ICRA), Montreal, QC, Canada, May 2019, pp. 102–108.

[10] A. A. Stanley, K. Hata and A. M. Okamura, "Closed-loop shape control of a Haptic Jamming deformable surface," *2016 IEEE International Conference on Robotics and Automation (ICRA)*, Stockholm, 2016, pp. 2718-2724.

[11] H. Schnadelbach, A. Irune, D. Kirk, K. Glover and P. Brundell, "ExoBuilding: Physiologically driven adaptive architecture", *ACM Trans. Comput. Interact. Artic.*, vol. 19, no. 4, 2012.

[12] V. M. Shakhin and T. V. Shakhina, "Waves on the Water Surface-Mathematical Models-Part 1," *Journal of Ocean and Climate Systems: Science, Technology, and Impacts*, vol. 6, no. 3, pp. 113–135, 2015.

[13] Y. Ng and S. Park, "Analysis and Realization of Ocean Wave Surface by Utilizing Matlab," in *The Journal of the Korea institute of electronic communication sciences*, 2010.

[14] M. Finch, "Chapter 1: Effective Water Simulation from Physical Models," in GPU Gems, ch. 1. [Online]. Available: https://developer.nvidia.com/sites/all/modules/custom/gpugems/books/PUGems/gpugems_ch01.html

[15] J. Merino, "Continuum Robotic Surface: Forward Kinematic Analysis and Implementation," M.S. thesis, Clemson Univ., Clemson, SC, 2013.

[16] Coastal Data Information Program. [Online]. Available: https://cdip.ucsd.edu/

[17] H. Mitsuyasu and S. Mizuno, "Directional Spectra of Ocean Surface Waves", *Int. Conf. Coastal. Eng.*, vol. 1, no. 15, p. 18, Jan. 1976.

[18] Salingaros, N. "The Biophilic Index Predicts Healing Effects of the Built Environment," *Journal of Biourbanism*, Volume 8, No.1, pp. 13-34, 2019.